Petroleum Science 23 (2026) 1348–1359

Contents lists available at ScienceDirect

Petroleum Science

journal homepage: www.keaipublishing.com/en/journals/petroleum-science

Original Paper

Investigating residual oil distribution and CO_2-EOR mechanisms in sand-conglomerate reservoirs using integrated CT and NMR techniques

Jun-Rong Liu [a,b], Run-Dong Gong [a,b], Deng-Feng Zhang [a,b,c], Wen-Yue Sun [a,b], Kai-Ning He [a,b], Shu-Yang Liu [a,b,*]

[a] School of Petroleum Engineering, China University of Petroleum (East China), Qingdao, 266580, Shandong, China
[b] Key Laboratory of Unconventional Oil & Gas Development, China University of Petroleum (East China), Qingdao, 266580, Shandong, China
[c] CNPC Engineering Technology Research Co., Ltd., Tianjin, 300451, China

ARTICLE INFO

Article history:
Received 18 September 2025
Received in revised form
3 November 2025
Accepted 28 November 2025
Available online 4 December 2025

Edited by Meng-Jiao Zhou

Keywords:
Sand-conglomerate reservoir
Multiscale
Shielding effect
Bypassed oil
CO_2-EOR

ABSTRACT

Sand-conglomerate reservoirs, comprising cemented sand grains and gravels, exhibit strong heterogeneity and complex flow behavior, which often result in poor sweep efficiency and low recovery during waterflooding. To enhance oil recovery, a clear understanding of residual oil distribution and the enhanced oil recovery (EOR) mechanisms is essential. This study employed Nuclear Magnetic Resonance (NMR) and Computed Tomography (CT) scanning to investigate the distribution of residual oil after waterflooding and to evaluate the EOR mechanisms of CO_2 flooding, CO_2-water-alternating-gas (CO_2-WAG) flooding, and CO_2 intermittent injection. Results show that the residual oil is predominantly "bypassed oil" trapped in macropores behind coarse gravels, with macropores accounting for 77.6% of the total residual oil. This is primarily due to gravel-induced shielding and flow bypassing, which significantly reduce sweep efficiency. All three CO_2 injection strategies effectively mobilize "bypassed oil", and intermittent CO_2 flooding achieves a higher CO_2-oil displacement efficiency than the other two. During intermittent CO_2 flooding, CO_2 not only partially extracts oil from the dominant channels but also dissolves into the "bypassed oil", causing oil to swell, enter the flow channel and then be produced. Additionally, increasing soaking time and cycle number can effectively improve the performance of this strategy. Extending soaking time enhance the contact between CO_2 and "bypassed oil", which is a key EOR mechanism. However, the incremental recovery diminishes with longer soaking time, potentially reducing overall operational efficiency. Thus, optimizing the operational parameters of these strategies requires further investigation.

1. Introduction

Sand-conglomerate reservoirs are widely distributed in China, the United States, Canada, Brazil, and Australia, and have become important targets for unconventional oil and gas development (Cronin and Kidd, 1998; Jia et al., 2017, 2018; Wang et al., 2020; Zhang et al., 2023). Formed mainly in high-energy depositional settings such as fluvial systems and alluvial fans, they contain mixed gravels and sands and commonly undergo strong compaction and cementation, leading to poor preservation of primary porosity (Clarke, 1979; Blatt et al., 1980). According to the Udden–Wentworth grain-size scale, gravels are classified as very fine (2–4 mm), fine (4–8 mm), medium (8–16 mm), and coarse (16–32 mm) classes (Udden, 1914; Wentworth, 1922). Compared with conventional sandstones, sand-conglomerate reservoirs exhibit complex genesis, pronounced heterogeneity, diverse pore structures, and large variability in storage and flow properties, which together complicate exploration and development (Xu et al., 2011; Zhang et al., 2023, 2025a).

Waterflooding remains the dominant development strategy, and numerous laboratory studies have investigated its performance. Liu et al. (2020) showed that the complex pore architecture in sand-conglomerates tends to cause early water breakthrough

* Corresponding author.
E-mail address: liu.shuyang@upc.edu.cn (S.-Y. Liu).
Peer review under the responsibility of China University of Petroleum (Beijing).

https://doi.org/10.1016/j.petsci.2025.11.047

(BT), limited sweep, and low ultimate recover. However, that work did not resolve the microscopic distribution of residual oil. Using NMR, Xu et al. (2011) reported preferential mobilization of macropores during waterflooding, with meso- and micro-pores contributing most to recovery. Yet their cores exhibited unimodal T_2 and relatively simple grain-size architecture and failed to capture the specific role of coarse gravel. As a result, the spatial distribution of residual oil in sand-conglomerates remains poorly resolved, limiting guidance for optimizing or transforming displacement strategies.

Moreover, in sand-conglomerate reservoirs, waterflooding is cost-effective but risks reservoir damage and typically achieves only limited sweep (Du et al., 2020; Zhao et al., 2024). In contrast, CO_2 injection shows strong EOR potential in sand-conglomerate reservoirs while also enabling CO_2 storage (Du et al., 2020; Raza et al., 2022; Zhou et al., 2024; Liu et al., 2025b). Its mechanisms include oil swelling, viscosity and density reduction, interfacial-tension lowering, and extraction of light hydrocarbons (Arshad et al., 2009; Ghasemi et al., 2017; Zhou et al., 2019; Song et al., 2024). Working with full-diameter cores, Han et al. (2018) found that even when waterflooding had established flow channels, CO_2 can still mobilize residual oil via diffusion-dominated mass transfer. Zhang et al. (2025a) and Tan et al. (2025) further indicated that microscopic heterogeneity is a primary control on CO_2 sweep efficiency. However, the pore-scale mechanisms in conglomerates remain insufficiently clarified. Du et al. (2020) employed NMR-based *in situ* monitoring to demonstrate the feasibility of CO_2 injection and the effective mobilization of micro- and mesopore oil through $scCO_2$–oil miscibility, but it failed to clarify how coarse gravel affects the underlying EOR mechanisms. Moreover, Kim et al. (2018) noted that the spatial distribution of clastic particles in conglomerates leads to distinct CO_2 storage behaviors, underscoring the non-negligible role of gravel. Overall, the impact of coarse gravel on fluid flow and EOR mechanisms during CO_2 injection remains insufficiently understood.

Monitoring fluid transport within core samples primarily relies on two key technologies: low-field NMR and X-ray Computed Tomography (CT) (Wei et al., 2019; Li et al., 2020, 2024; Xu et al., 2020; Cai et al., 2021). NMR excels at quantifying oil mobilization within different pore sizes, thereby revealing microscopic displacement patterns (Wei et al., 2019). However, due to inherent limitations such as resolution, internal field gradients, and signal overlap, NMR cannot accurately map the spatial distribution of the oil phase within the core (Guo et al., 2020). On the other hand, CT technology enables the spatial localization of fluids. High-resolution CT can resolve pore structures and identify local trapped phases, but its field of view is extremely limited, rendering it unsuitable for characterizing large core samples (Cnudde and Boone, 2013). Conversely, while industrial CT can scan large cores and clearly identify gravels in sand-conglomerate samples, its lower resolution precludes a precise depiction of pore-scale fluid mobilization (Wildenschild and Sheppard, 2013). Therefore, a fundamental conflict arises when using a single technology to comprehensively characterize residual oil in highly heterogeneous reservoirs like sand-conglomerates: NMR lacks spatial information, while CT faces an inherent trade-off between resolution and sample size.

To bridge this gap, this study integrates CT and NMR technologies to leverage their complementary strengths, with CT for macro-scale spatial localization of gravels and fluids and NMR for quantitative analysis of oil mobilization within microscopic pores. Through this cross-validation and informational synergy, the residual oil distribution characteristics and flow-path evolution in sand-conglomerate reservoirs can be multi-scale investigated from core to gravel to pore. Additionally, this work systematically compares continuous CO_2 flooding, CO_2-WAG, and intermittent CO_2 flooding, revealing their distinct mobilization efficiencies and dominant EOR mechanisms in the presence of coarse gravel. Finally, sensitivity analyses of soaking time and cycle number further quantify their impact on recovery and provide guidance for field-scale optimization.

2. Materials, apparatus, and experimental schemes

To systematically elucidate residual-oil distribution and the EOR mechanisms under different displacement strategies in a sand-conglomerate reservoir, a suite of core-flooding experiments was designed and conducted using actual cores and crude oil. This section first described the petrophysical properties of the experimental materials, then introduced the apparatus of low-field NMR for *in situ* monitoring of fluid transport and CT scanning for localizing the spatial distribution of residual oil, and last depicted the experimental schemes for different flooding strategies.

2.1. Materials

A standard sand-conglomerate core (Ø 38 mm, H 50 mm) was prepared from Block X, Tianjin, as shown in Fig. 1. While a single core cannot be representative of the reservoir at the macro-scale, the gravels it contains are one of the most widespread and flow-critical structures within such formations. These gravels represent a typical unit of microscopic heterogeneity. By utilizing the core, this study specifically focused on the controlling influence of gravel on the local flow field and residual oil distribution, thereby providing a fundamental yet crucial insight for understanding reservoir-scale flow behavior. Permeability and porosity, measured using a steady-state gas permeameter and a helium porosimeter, were 10.12 mD and 15.3%, respectively.

Heavy water (D_2O, 99.8% purity; 1H-NMR silent) served as the injected water, and CO_2 (99.9% purity) was used as the injected gas. The crude oil was degassed field oil with a viscosity of 5.93 mPa s at 70 °C, and its composition is presented in Table 1.

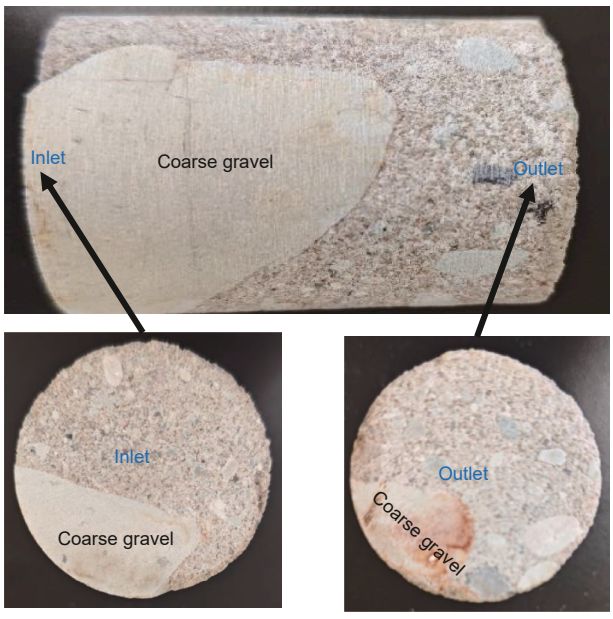

Fig. 1. Sand-conglomerate core.

Table 1
Component of crude oil.

Components	Mass fraction, %
C_1–C_6	1.6
C_6–C_{12}	21.9
C_{13}–C_{20}	23.3
C_{21}–C_{30}	24.1
C_{30+}	29.1

2.2. Apparatus

An *in situ* low-field NMR–assisted coreflooding system (Fig. 2) was assembled to characterize residual oil and to clarify EOR mechanisms in the sand-conglomerate core. The system was configured with four modules:

(1) Monitoring module is mainly consisted of a high-temperature, high-pressure *in situ* NMR analyzer (MesoMR12-060H-I, Suzhou Niumag; B0 = 0.30 ± 0.03 T).
(2) Injection module employed a high-precision plunger pump (Vindum Instruments, flow-rate accuracy 1×10^{-5} mL/min, pressure max: 80 MPa) and a high-pressure intermediate accumulator (Pressure max: 50 MPa).
(3) Flooding module is mainly consisted of a non-magnetic core holder coupled to a thermostatic circulation system.
(4) Collection module employs a back-pressure regulation system (Xiongchuan; accuracy 0.01 MPa; pressure max: 27.6 MPa) and a gas–liquid separator.

The NMR analysis involved two complementary measurements. Oil-phase distribution maps were acquired with the MRI (magnetic resonance imaging) module to visualize macroscale fluid changes and sweep efficiency. Simultaneously, T_2 distributions were obtained via the CPMG sequence to resolve pore-scale fluid mobilization. To enhance the interpretation of MRI data, the raw grayscale images, which represent proton signal intensity, were post-processed. Specifically, using the Pcolor function within the Niumag software, all images were rendered into pseudocolor by applying a standardized Jet colormap.

To establish a quantitative relationship between the T_2 signal intensity and fluid volume, a standard calibration experiment was performed. First, oil samples with precise volumes of 1, 2, 3, 4, and 5 mL were prepared in individual sample tubes and their T_2 spectra were measured using parameters identical to those in the core experiments. Subsequently, a linear regression analysis was conducted with the total T_2 signal intensity as the *Y*-axis and the corresponding oil volume as the *X*-axis (Fig. 3). This calibration is

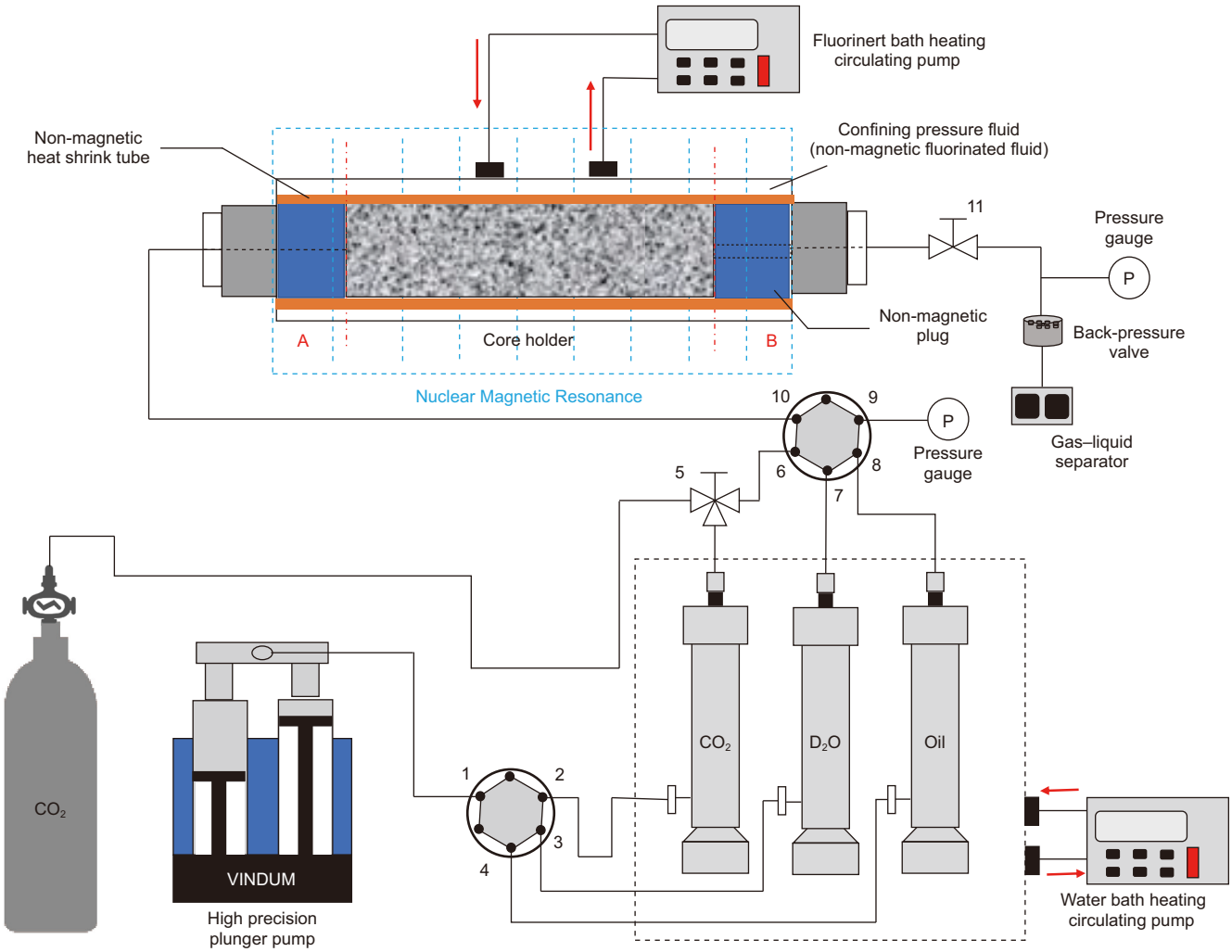

Fig. 2. Sand-conglomerate displacement experiment system.

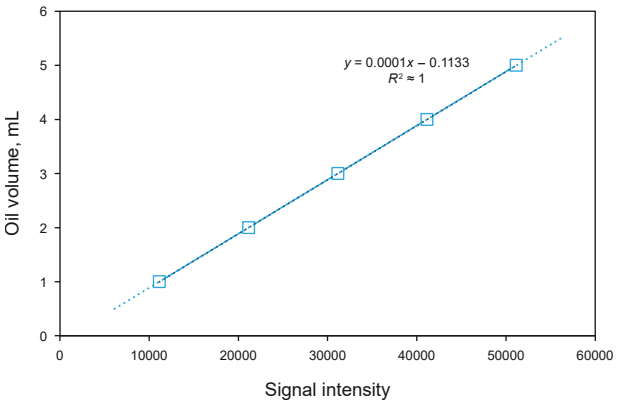

Fig. 3. Relationship curve between oil content and NMR signal intensity.

based on a fundamental principle of NMR: the total integrated signal intensity of the T_2 spectrum is directly proportional to the total number of hydrogen protons in the fluid (as well as the fluid volume), and is largely unaffected by the fluid's environment (e.g., pore size or bulk state), although the distribution of T_2 relaxation time is influenced by the pore structure (Coates et al., 1999). The resulting linear regression (Eq. (1)) yielded a correlation coefficient (R^2) of almost 1, which not only confirms the linear correspondence between signal intensity and oil volume but also demonstrates the high stability and reliability of the experimental system.

$$V = 0.0001Q - 0.1133 \quad (1.)$$

where V represents the oil volume, mL; Q represents the total NMR signal intensity.

An equipment of CT scanning (Nanovoxel 3000, Sanying Precision Instruments Co., Ltd., China) was employed to delineate the pore-scale sweep behavior in the sand-conglomerate, enabling the identification of pore-scale heterogeneity, and the precise localization of residual oil distribution.

2.3. Experimental schemes

A baseline waterflood was first performed to characterize the distribution of residual oil and flow behavior in the sand-conglomerate core. Building on this basis, CO_2 flooding, CO_2-WAG, and intermittent CO_2 flooding were subsequently conducted to elucidate EOR mechanisms under different development strategies. Finally, the schemes for effects of soaking time and cycle number on CO_2-injection performance were set to optimize operating parameters and enhance recovery. Detailed experimental schemes and parameter settings are summarized in Table 2.

All flooding experiments were monitored in real-time using the *in-situ* NMR instrument. The experiments were conducted under consistent conditions, with a constant injection rate of 0.5 mL/min, a confining pressure of 25 MPa, and a back pressure of 20 MPa. Throughout the entire displacement process, the pressure drops across the core remained minimal, fluctuating by less than 0.3 MPa. This indicates that the maximum inlet pressure was approximately 20.3 MPa, which is well below the CO_2-oil minimum miscibility pressure (MMP) of 23.1 MPa, confirming that all CO_2 injection occurred under immiscible conditions. The detailed procedures are described below, using the waterflooding stage (Scheme 1) as an example:

(1) Core preparation
   ① The core was alternately cleaned with toluene and ethanol three times and then vacuum-dried at 105 °C for 24 h.
   ② At a constant flow rate of 0.05 mL/min, the core were first saturated with heavy water (D_2O) and then with crude oil at the same rate until the produced water cut fell below 0.1%; the irreducible (bound) water saturation was calculated accordingly.
   ③ After establishing the initial fluid saturation, the oil-saturated core was scanned again via CT to visualize the initial oil distribution.

(2) Flooding experiment
   ① The fully saturated core was placed into the *in situ* NMR core holder. To simulate reservoir stress conditions, a confining pressure of 25 MPa and a back pressure of 20 MPa were applied.
   ② Oil was then injected at 0.5 mL/min to pressurize the system and fill the downstream pipeline, ensuring a single-phase fluid environment before the flooding experiment.
   ③ The system was allowed to equilibrate for 12 h under these static conditions.
   ④ Under a back pressure of 20 MPa, flooding (waterflooding for Scheme 1) was performed at 0.5 mL/min.
   ⑤ T_2 and MRI maps were acquired every 0.1 PV of injected D_2O.
   ⑥ The flooding was terminated when a cumulative injection of 5 PV was reached and no further increase in recovery was observed. A CT scan was then performed to map the residual-oil distribution.

After residual oil had been established by waterflooding, CO_2 flooding, CO_2-WAG, and intermittent CO_2 flooding were conducted flowing the procedure (2). The experiment was terminated after 5 PV of CO_2 injected, as shown in Table 2.

3. Results and discussion

3.1. Residual oil distribution during waterflooding

To investigate the residual oil distribution during waterflooding in the sand-conglomerate core, this section employed MRI technology to monitor oil phase migration in real time. The experimental parameters are listed as Scheme 1 in Table 2, and the corresponding results are presented in Fig. 4, in which blue indicates the aqueous phase (weak signal), red denotes the oil (strong signal), and the black dotted line marks the gravel boundary. The results revealed that during waterflooding, the presence of gravel altered the flow path of water, destabilizing the advancing front and leaving substantial amounts of residual oil trapped behind the gravel. Notably, an apparent increase in the oil signal was observed within the coarse gravel between 0 and 1 PV injected. This phenomenon is a combined effect of the 2D projection imaging and fluid redistribution. Specifically, the NMR image is not a cross-sectional slice but a 2D projection of the total signal along the line of sight. During waterflooding, the flow path bypassed the coarse gravel, potentially squeezing oil from adjacent high-permeability regions into this area and causing localized accumulation. This local enrichment manifests as a slight increase in the total signal intensity for the region, which is considered a normal imaging artifact.

To further quantify the effect of waterflooding on oil recovery and investigate the microscopic activation mechanisms, the dynamic T_2 spectra during the displacement process was analyzed as

Table 2
Experimental schemes for the sand-conglomerate core.

Scheme	Strategy	Process	*n* (cycle number)	*t* (soaking time), min	Pressure, MPa	Injection rate, (mL/min)	Purpose
1	Waterflooding	W(5)	\	\	20	0.5	Distribution characteristics of remaining oil. Flow behavior
2	CO_2 flooding	W(5)→G(5)	\	\	20	0.5	EOR
3	CO_2-WAG	W(5)→G(1) →[W(1)→G(1)] × 4	4	\	20	0.5	mechanism of
4	Intermittent CO_2 flooding	W(5)→G(1) →[S(t)→G(1)] × 4	4	30	20	0.5	different CO_2-injection strategies
6–10	Intermittent CO_2 flooding	W(5)→G(1) →S(t)→G(4)	1	0, 10, 30, 240, 720, 2880	20	0.5	Soaking time
11–20	Intermittent CO_2 flooding	W→G(1) →[S(t)→G(1)] × *n*	1–10	30	20	0.5	Cycle number

Note: W and G denote waterflooding and CO_2 injection, respectively, in which the number in parentheses is the injected volume, PV, and S denotes soaking, in which the number in parentheses is the soaking time, min). PV represents pore volume.

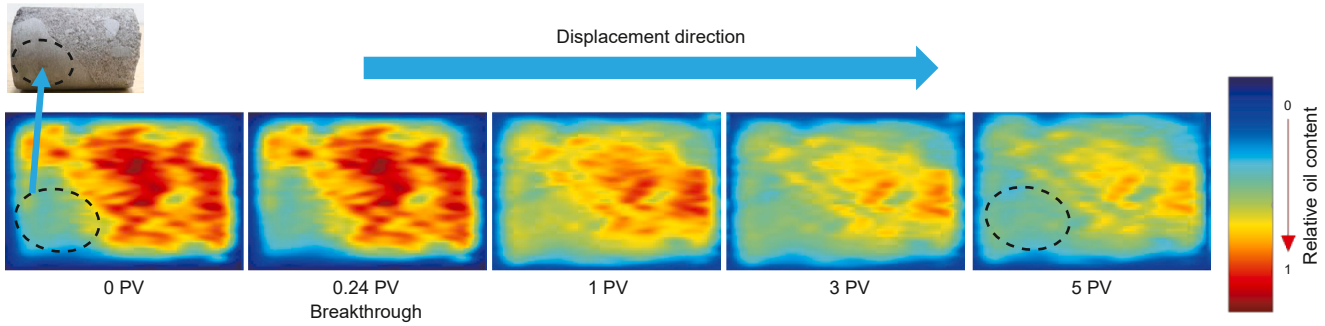

Fig. 4. Dynamic oil distribution during waterflooding.

shown in Fig. 5. Pores were grouped into three classes, including micropores (0.001–1 ms), mesopores (1–100 ms), and macropores (100–10,000 ms). The signal at initial state (0 PV) is mainly distributed in the relaxation time region larger than 1 ms, indicating that the crude oil primarily resides in mesopores and macropores, with a minimal contribution from micropores. This distribution is dictated by the inherent physical structure of the 10.12 mD sand-conglomerate core, which is dominated by meso- and macro-pores. Thus, the analysis of the residual oil mechanism focuses on the dynamic recovery from both the core on a macroscopic scale and the meso- and macro-pores on a microscopic scale. In contrast to the conventional capillary trapping mechanism, residual oil after waterflooding was primarily located in macropores but not micropores in this work.

Based on the signal conversion Eq. (1), the overall oil recovery (R) in flooding experiments can be characterized as:

$$R = \frac{S_0 - S_i}{S_0} \times 100\% \tag{2}$$

where S_0 and S_i are the T_2 signal for the entire core at initial time and after i PV injection, respectively. As shown in Fig. 6, the overall recovery reaches 52% after 5 PV of displacement, leaving nearly half of the oil trapped within the core.

To further characterize oil recovery behavior in different size of pores, the pore-scale oil recovery (R_p) was calculated as

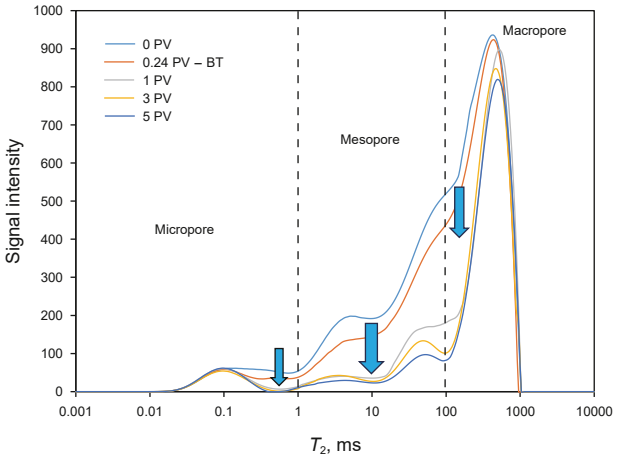

Fig. 5. T_2 curve in the waterflooding.

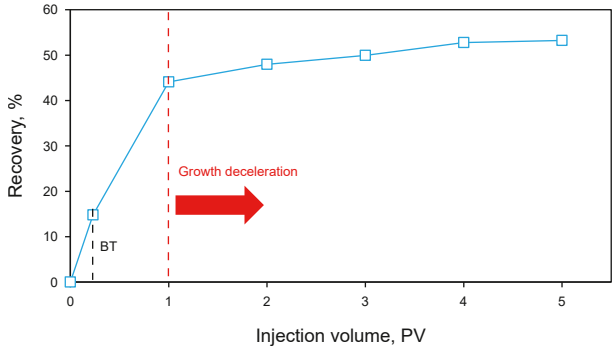

Fig. 6. The overall oil recovery during waterflooding.

$$R_p = \frac{S_0^p - S_i^p}{S_0^p} \times 100\% \quad (3)$$

where S_0^p and S_i^p are the T_2 signal for the pore at initial time and after i PV injection, respectively. The results show that mesopores were mobilized most efficiently, with a recovery of 82.0%, which is 1.9 and 2.5 times higher than that of micropores and macropores, respectively, as shown in Fig. 7. In theory, macropores should be easier to mobilize due to their lower capillary resistance (Beven and Germann, 2013; Yang et al., 2025). However, the experimental recovery from macropores was lower than that from both micro- and mesopores. Furthermore, calculations based on the curve at 5 PV in Fig. 5 show that the residual oil in macropores accounted for 77.6% of the total residual oil. The results reveal a mobilization pattern that deviates sharply from that observed in conventional sandstone reservoirs (Wei et al., 2020, 2023; Zhang et al., 2022). In conventional reservoirs, the oil within macropores (i.e., "free fluid") is considered the most mobile and is expected to be produced preferentially (Liu et al., 2025a). Conversely, the results in these experiments different from former researches is attributed to the strong macroscopic heterogeneity of the sand-conglomerate core. The uneven distribution of coarse gravel alters waterflood flow paths, resulting in inefficient sweep of macropores and leaving a substantial volume of oil unswept.

To investigate this anomalous oil mobilization behavior, the high-resolution X-ray CT was employed to further resolve the three-dimensional (3D) distribution of residual oil. The core was reconstructed in 3D from 2600 slices to characterize the internal structure of core sample as shown in Fig. 8(a). Subsequently, individual gravel particles were digitally isolated from this model using a watershed segmentation algorithm (Fig. 8(b)). The results clearly reveal the significant heterogeneity of core sample. Gravels are distributed widely, and their arrangement is non-uniform, with a notable concentration of coarse gravels in the lower-left region and smaller gravels scattered throughout the remaining volume. This structural arrangement is critical, as the coarse gravels disrupt flow paths on a much larger scale than the smaller ones, forcing the fluid into longer and more tortuous detours. This, in turn, is expected to create a highly non-uniform flow field within the core.

To verify the retention mechanism of "bypassed oil", the oil distribution around the gravels was analyzed before and after flooding in a representative region. Because the entire core volume could not be fully characterized due to computational limits, the lower-left coarse-gravel region was selected as a typical area for detailed investigation of residual oil distribution and mobilization characteristics, as shown in Fig. 8(c) and (d).

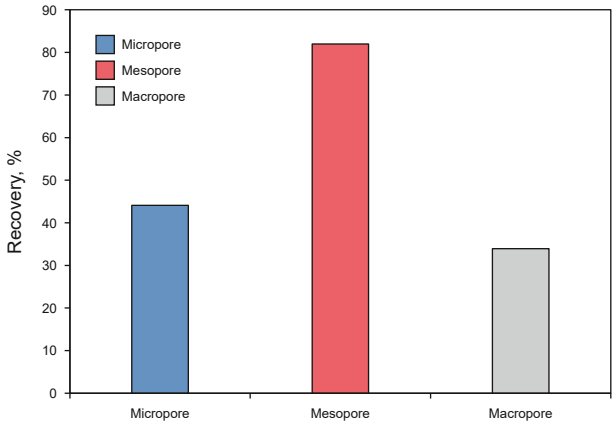

Fig. 7. Pore-scale oil recovery during waterflooding.

As shown in Fig. 9, substantial oil remained after waterflooding, and the local oil recovery in the analyzed region was only 27.1%. To visualize the impact of coarse gravel on residual-oil distribution, this section further processed the CT data to retain only the coarse gravel and adjacent residual oil (Fig. 10). The results show that 56% of the residual oil resides on the lee side of the coarse gravel. This spatial distribution provides a powerful cross-validation for the preceding NMR results (Fig. 5), which revealed that residual oil was predominantly located in macropores, but cannot resolve the specific 3D locations of these pores. The CT visualization in Fig. 10 precisely bridges this gap. By integrating the statistical finding from NMR (that residual oil is concentrated in macropores) with the spatial observation from CT (that residual oil accumulates in the shielded regions behind gravel), it can be inferred that the oil trapped in macropores is mainly located at the rear of coarse gravel. This reveals that the dominant mechanism for significant oil trapping in this type of reservoir is not the conventional capillary trapping that primarily affects micropores. Instead, it is a "shielding effect" induced by the coarse gravel during displacement. This effect causes water to bypass the gravel, failing to efficiently sweep the large pore space behind it and thus generating "bypassed oil".

These findings clarify the critical influence of coarse gravel on sweep efficiency and residual-oil distribution, highlighting the significant volume of "bypassed oil" trapped by the shielding effect. Therefore, to address this specific issue and explore optimal methods for EOR, three different CO_2 injection strategies were subsequently implemented and evaluated.

3.2. Effects and mechanisms of CO_2 injection on enhanced oil recovery

To reduce the residual oil after waterflooding, three CO_2 injection strategies were conducted: continuous CO_2 flooding, CO_2-WAG, and intermittent CO_2 flooding. The experimental parameters and procedures are summarized as Schemes 2–4 in Table 2. MRI was used throughout to visually assess the mobilization performance of each strategy (Fig. 11). Following waterflooding, all CO_2 injection strategies were shown to significantly reduce residual oil. However, a small amount of residual oil remained concentrated around the gravel, as highlighted by the yellow circles. Among the strategies, both CO_2-WAG and intermittent flooding mobilized "bypassed oil" around the coarse gravel more effectively than continuous flooding.

To quantify how CO_2-injection strategies affected recovery, the NMR T_2 distributions for each strategy were compared in Fig. 12. The signal intensity in the macropore region showed a pronounced decrease in intensity, whereas the signals from micro- and mesopores changed little. The decrease in macropore signal intensity became more pronounced, progressing from continuous CO_2 flooding to CO_2-WAG, and was greatest under intermittent CO_2 flooding. Using Eq. (2), the overall oil recovery was calculated and shown in Fig. 13. The overall recoveries of CO_2 flooding, CO_2-WAG, and intermittent CO_2 flooding were 62.9%, 67.4%, and 69.6%, respectively. Compared with water flooding, CO_2-WAG and intermittent CO_2 flooding increased the overall recovery by 14.2% and 16.4%, reaching 1.5 times and 1.7 times that of CO_2 flooding.

To elucidate the pore-scale mechanisms of different displacement strategies, the pore-scale recovery for each pore class were calculated using Eq. (3). As shown in Fig. 13, micropores and mesopores showed only minor gains, whereas macropores dominated the improvements, compared to waterflooding as shown in Fig. 5. Macropore recovery rose by 16.5%, 24.4%, and 28.9% under

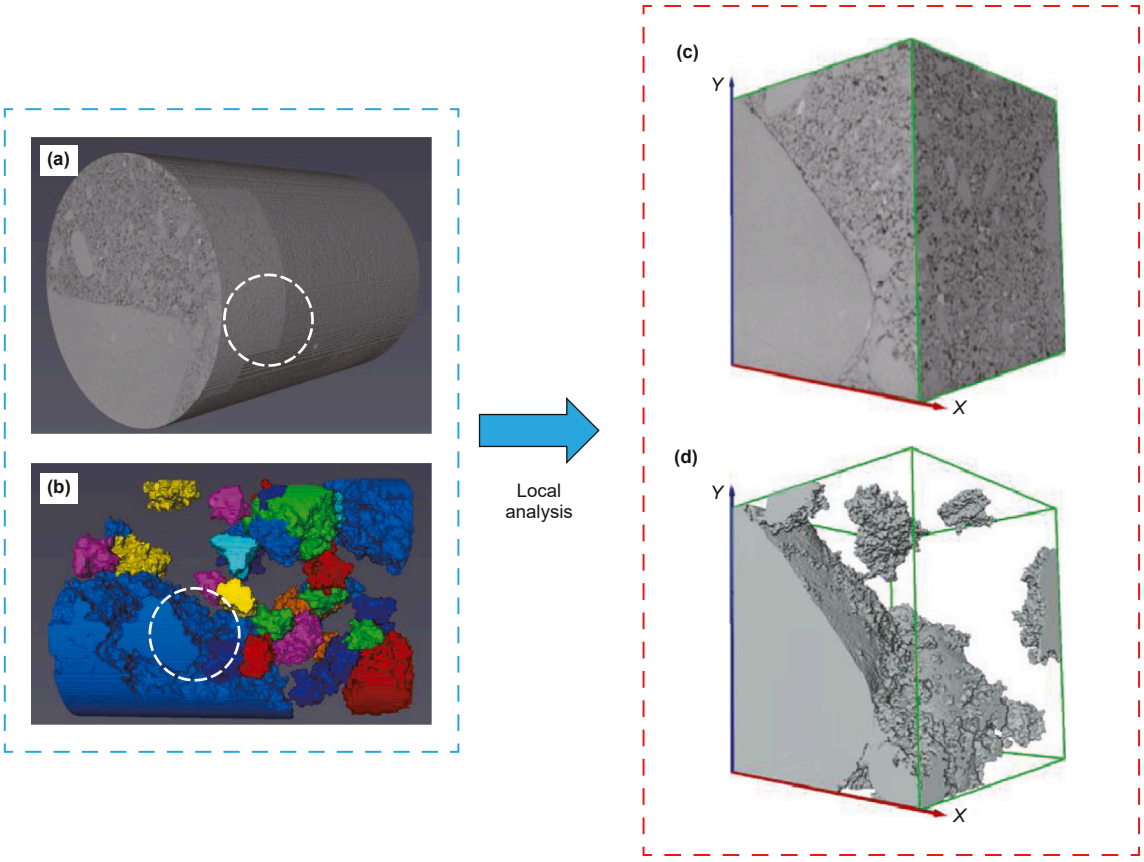

Fig. 8. Particle size analysis and representative region selection after 3D core reconstruction (white circle indicates extraction location): **(a)** 3D reconstruction; **(b)** gravel distribution; **(c)** segmented core; **(d)** coarse gravel.

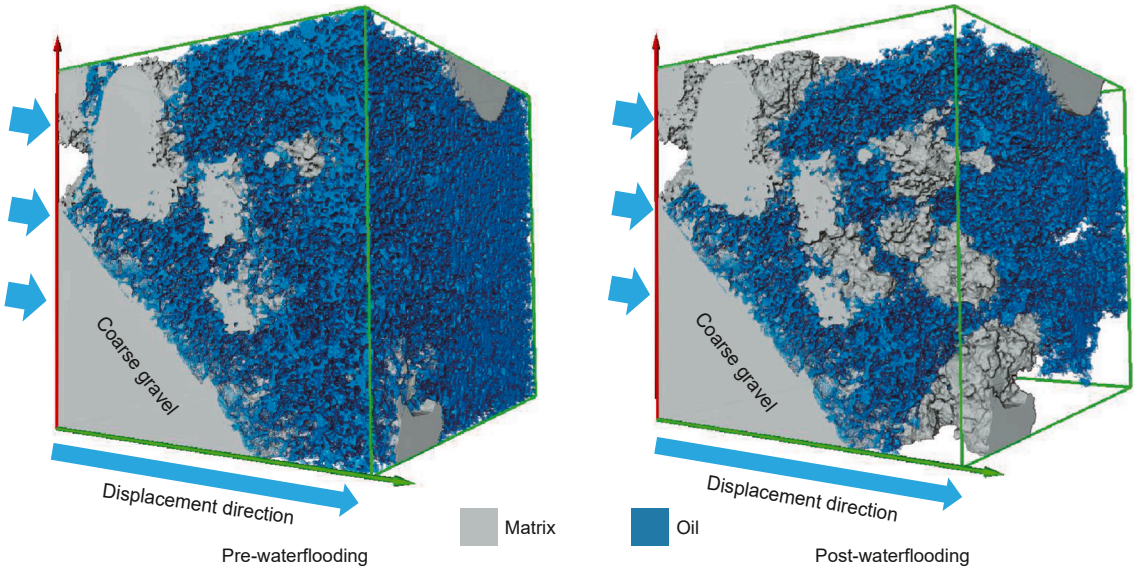

Fig. 9. Oil distribution pre- and post-waterflooding.

continuous flooding, CO_2-WAG, and intermittent flooding, respectively, with the final recovery reaching 1.57, 1.85, and 2.12 times that under waterflooding. Thus, in the sand-conglomerate core, the EOR effect of CO_2 injection mainly attributed to improved macropore mobilization, with intermittent CO_2 flooding being the most effective.

Waterflooding in such a heterogeneous core is fundamentally limited by bypass flow. As shown in Fig. 14, the injected water quickly establishes preferential channels in the non-gravel regions, while the oil located in the "shadow regions" downstream of the gravels remains almost entirely unswept, creating pockets of "bypassed oil". CO_2 injection fundamentally alters this dynamic. In

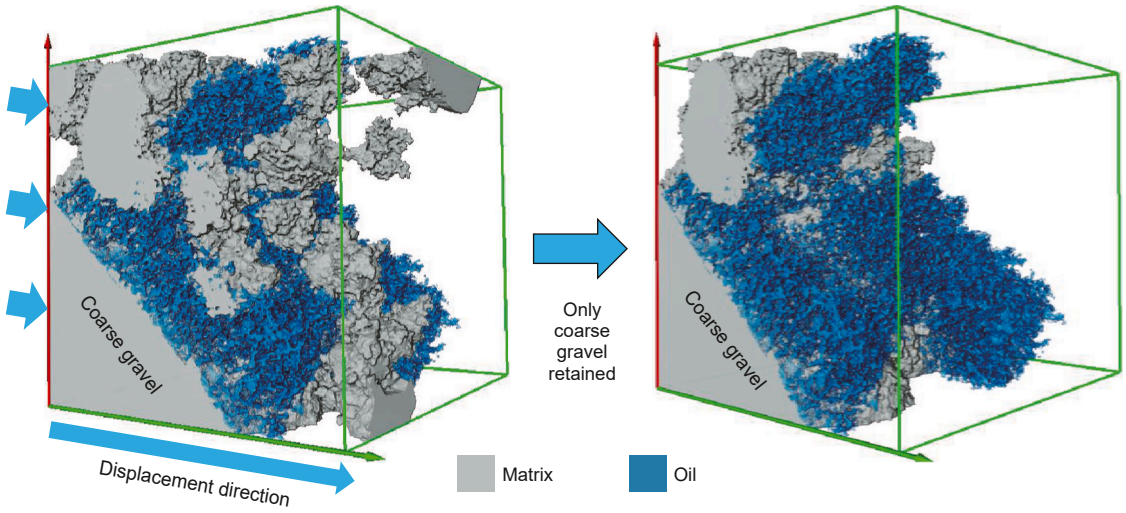

Fig. 10. CT reconstruction of the coarse gravel with adjacent residual oil.

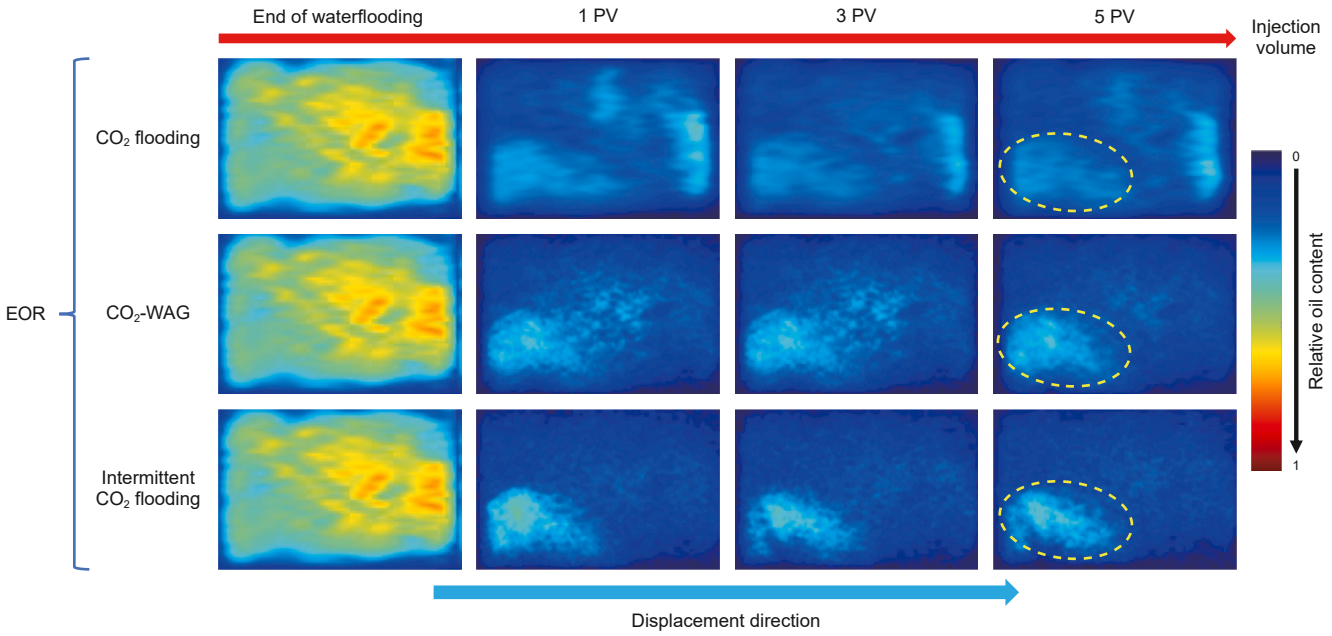

Fig. 11. Dynamic distribution of crude oil under different CO_2-injection strategies.

contrast to water, CO_2 can diffuse into the trapped oil, and mobilize it through mechanisms of swelling, viscosity reduction, and component extraction.

Building on this, CO_2-WAG alternates water slugs to block established preferential channels and suppress viscous fingering (Ramachandran et al., 2010), which further broadens sweep and mobilizes "bypassed oil". Intermittent CO_2 flooding introduces soaking periods after injection, which prolongs CO_2–oil contact, enhances diffusion (Chen et al., 2022), and allows "bypassed oil" in macropores to swell into flow paths. This mechanism markedly improves recovery. Both CO_2-WAG and intermittent CO_2 flooding attenuate the shielding effect of coarse gravel, thereby significantly mobilizing "bypassed oil".

While both strategies proved effective, intermittent CO_2 injection achieved a higher recovery. The physical barrier formed by water slugs in the CO_2-WAG strategy is inherently transient, as the high-mobility CO_2 rapidly re-penetrates the preferential channels, causing the blockage to fail. In contrast, intermittent CO_2 flooding leverages diffusion during the soaking period to directly "activate" the bypassed oil from within through swelling and viscosity reduction. Additionally, CO_2-WAG can be operationally complex, costly, and prone to corrosion in field applications (Iyer et al., 2022; Koray et al., 2025). The simpler operational profile and higher recovery efficiency of intermittent CO_2 flooding thus make it a more suitable choice for sand-conglomerate reservoirs.

Notably, the soaking time and the number of soaking cycles have a significant impact on the final recovery (Iraji et al., 2015; Pu et al., 2016; Liu et al., 2022). The next section conducts a sensitivity analysis of these key parameters to guide field implementation.

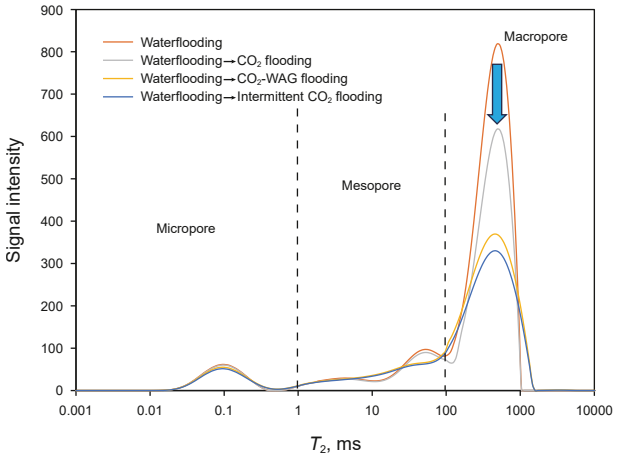

Fig. 12. T_2 for different displacement strategies.

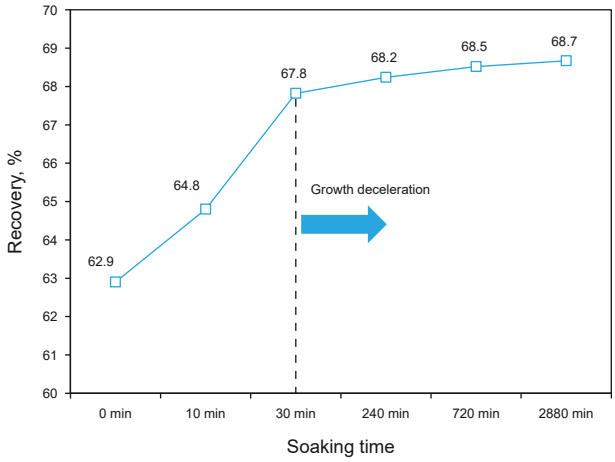

Fig. 15. The overall oil recovery versus soaking time.

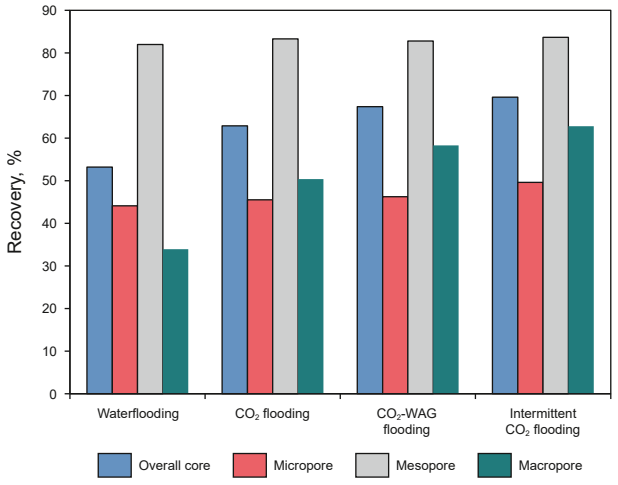

Fig. 13. The overall and pore-scale recovery under different displacement strategies.

3.3. *Sensitivity analysis for intermittent CO_2 flooding*

To investigate the effect of soaking time on oil recovery in intermittent CO_2 flooding, a series of experiments (Schemes 6–10 as shown in Table 2) were conducted. After 5-PV waterflooding, 1 PV of CO_2 was injected to ensure sufficient contact, followed by intermittent CO_2 flooding. The overall oil recovery versus soaking time was quantified using T_2 analysis coupled with Eq. (2). As shown in Fig. 15, recovery increased with soaking time but with diminishing increments. Relative to no soaking (0 min), oil recovery increased by 4.9% at 30 min and 5.8% at 2880 min. Considering economic and time costs, a 30-min soak was deemed preferable.

To further clarify pore-scale mobilization, T_2 spectra at 0, 30, and 2880 min were analyzed (Fig. 16). From 0 to 30 min, the macropore signal decreased markedly, whereas the signals from micro- and mesopores changed little. However, from 30 to 2880 min, the amplitudes varied only slightly. Quantitative analysis indicates that with increasing soak time, pore-scale recovery from macropores rose more markedly, whereas recovery from micro- and mesopores increased only slightly, as shown in Fig. 17. At 2800 min, the macropore recovery reached 57.1%, only 2.0% higher than that at 30 min, yet it required approximately 96 times longer soaking. Prolonged soaking enhances CO_2 dissolution into

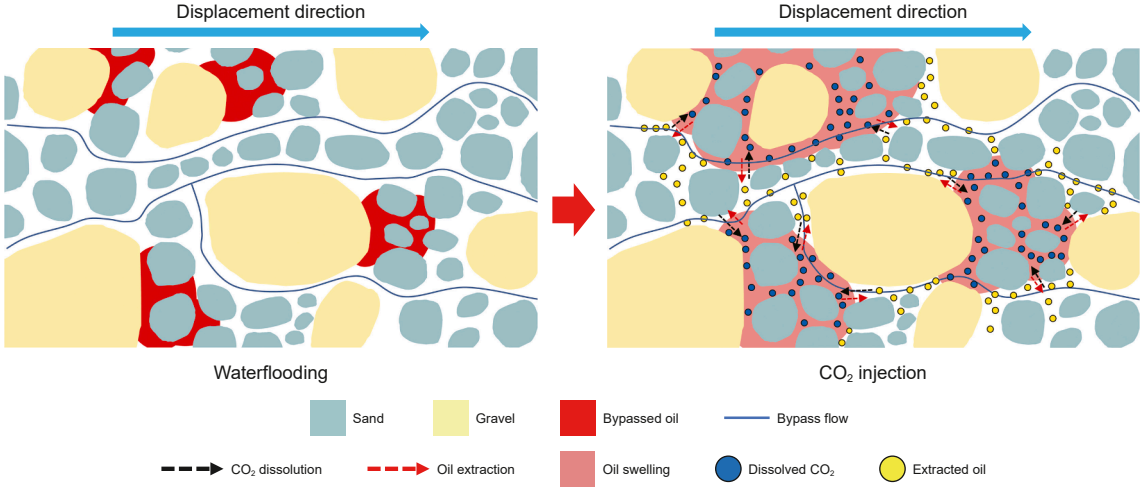

Fig. 14. Schematic of flow patterns during waterflooding and CO_2 injection flooding in the sand-conglomerate core.

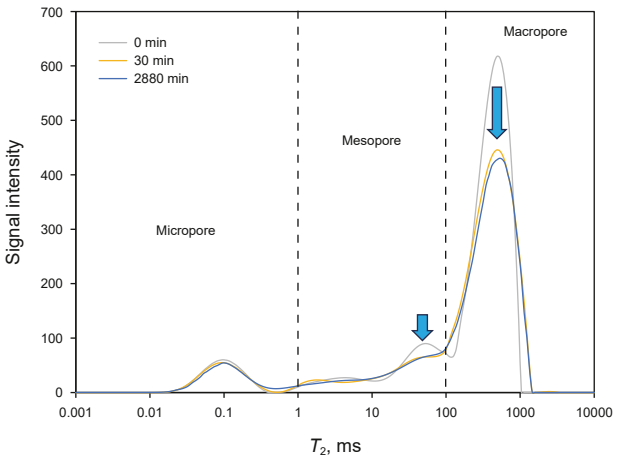

Fig. 16. T_2 curve for different soaking time.

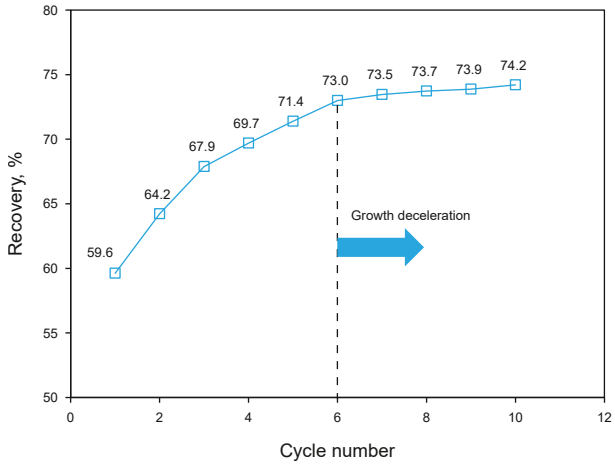

Fig. 18. The overall recovery versus number of soaking cycles.

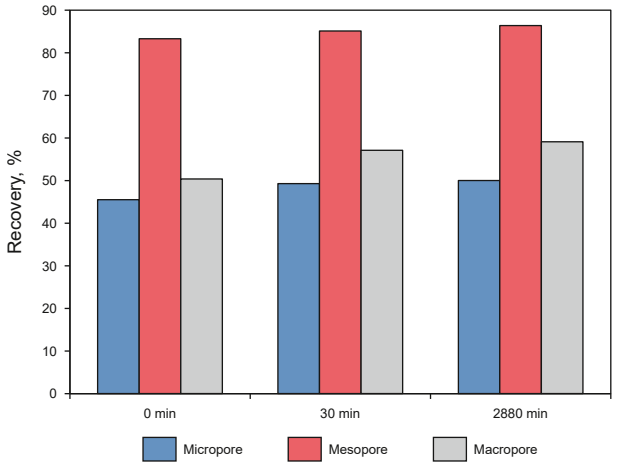

Fig. 17. Pore-sacle recovery for different soaking time.

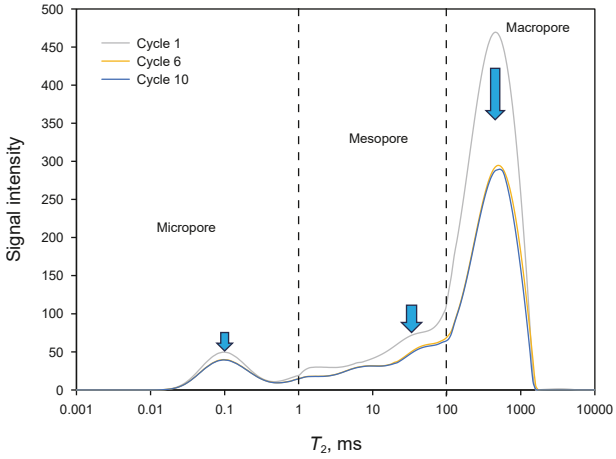

Fig. 19. T_2 curve for different cycle number.

oil, swelling of "bypassed oil" in macropores and CO_2 extraction. Initially, steep concentration gradients drive rapid CO_2 diffusion into the oil. As the oil approaches CO_2 saturation, the gradient weakens and diffusion slows (Rezk and Foroozesh, 2022; Luo et al., 2023; Zhang et al., 2025b). Consequently, oil swelling becomes negligible, and extraction efficiency declines. Excessively long soaking is therefore unnecessary.

To quantify the effect of cycle number on recovery, schemes 11–20 were conducted. Each cycle comprised a 30-min soak followed by the injection of 1 PV CO_2. This section acquired T_2 at the end of each cycle and computed recovery using Eq. (2) (Fig. 18). Recovery increased with cycle number, but the increments diminished after the 6th cycle. The 6th and 10th cycles yielded recovery of 73.0% and 74.2%, and a difference of only 1.2% indicated that six cycles represent the optimal scheme.

Pore-scale mobilization with increasing cycle number was further examined (Fig. 19). From the 1st to the 6th cycle, micropore and mesopore signals declined markedly, though mesopores exhibited smaller reductions. From the 6th to the 10th cycle, mesopore and macropore signals decreased only slightly. Quantitative results (Fig. 20) indicated that cumulative recovery ranked as macropores > micropores > mesopores, with gains of 21.9%, 10.0%, and 6.4%, respectively. Each cycle not only produced oil but also created new CO_2 storage space and flow pathways, altering

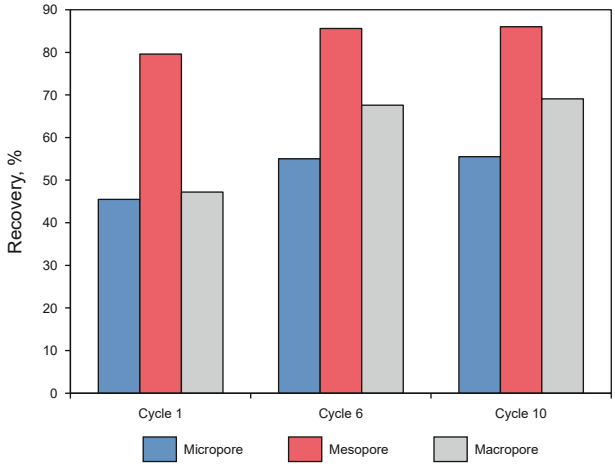

Fig. 20. Pore-scale recovery for different cycle number.

flow paths and allowing CO_2 to access previously unswept regions. With additional cycles, the readily mobilizable residual oil was progressively depleted, and both the swept volume and flow paths

approached saturation, resulting in minor incremental recovery beyond the 6th cycle.

A comparison of the injection schemes reveals the key to optimizing operational parameters. The findings show that in highly heterogeneous reservoirs like sand-conglomerates, both soaking time and cycle number are sensitive parameters for enhancing oil recovery. The core mechanisms are distinct: soaking mobilizes residual oil from "shielded regions" via diffusion, while multiple cycles expand the swept volume by reconfiguring the flow field. However, both approaches exhibit significant diminishing marginal returns. Therefore, this study emphasizes on a mechanistic level that field applications must optimize the combination of soaking time and cycle number through pilot tests and numerical simulations tailored to specific reservoir characteristics. This is essential to strike the optimal balance between maximizing recovery and ensuring economic viability by avoiding inefficient injection costs.

4. Conclusions

This work integrated core-flooding experiments on a sand-conglomerate core with NMR and CT imaging to conduct a multiscale characterization. The study focused on the rock-coarse gravel-pore residual-oil distribution after waterflooding and coarse gravel-induced bypassing and shielding effects. On this basis, this work systematically evaluated the mechanisms and performance of continuous CO_2 flooding, CO_2-WAG, and intermittent CO_2 flooding, and optimized the soaking time and number of cycles for the intermittent strategy, proposing a practical, operationally feasible, and optimal development scheme. The main conclusions are drawn as follows:

(1) The unusually high residual oil saturation after waterflooding underscores that oil retention in sand-conglomerate systems is not governed solely by classical capillary trapping. Instead, the spatial heterogeneity dominates fluid distribution, particularly through their control of preferential flow.
(2) The occurrence of residual oil within macropores originates from heterogeneity-induced flow partitioning rather than capillary trapping. The presence of coarse gravels induces preferential bypass flow, creating a shielding effect that isolates oil on the trailing side and reduces local sweep efficiency.
(3) CO_2-based flooding all significantly enhanced core-scale recovery in the sand-conglomerate core, with especially large gains in macropore recovery. This is because they attenuate the shielding effect of coarse gravel and effectively mobilize "bypassed oil".
(4) Intermittent CO_2 flooding achieved the highest recovery. Its advantage lies in the post-injection soaking, which enhances diffusion between CO_2 and the bypassed oil, driving this oil into flow paths and thereby maximizing swept volume and displacement efficiency.
(5) For intermittent flooding, both soaking time and cycle number are sensitive parameters that demonstrate diminishing marginal returns. Field applications should therefore optimize this combination to achieve the best balance between maximizing ultimate recovery and ensuring economic viability by avoiding inefficient, prolonged operations.

The primary limitation of this study is that the dynamic displacement process remains a "black box" reliant on indirect inference—namely, the cross-validation of NMR and CT data. To transition from inference to visualization, future research may pivot to microfluidic technology. By fabricating chips that replicate gravel-induced heterogeneity, it will become possible to directly observe CO_2 bypassing, diffusion, and oil mobilization. These micro-scale observations are crucial for quantitatively assessing the contributions of different EOR mechanisms and optimizing recovery strategies.

CRediT authorship contribution statement

Jun-Rong Liu: Writing – review & editing, Validation, Supervision, Investigation, Funding acquisition, Formal analysis, Conceptualization. **Run-Dong Gong:** Writing – original draft, Visualization, Methodology, Investigation, Formal analysis, Data curation. **Deng-Feng Zhang:** Writing – original draft, Visualization, Investigation. **Wen-Yue Sun:** Writing – review & editing, Supervision, Funding acquisition. **Kai-Ning He:** Investigation, Data curation. **Shu-Yang Liu:** Validation, Supervision, Resources, Funding acquisition.

Declaration of interest

No conflict of interest exists regarding the submission of this manuscript. All authors have approved the manuscript for publication. On behalf of my co-authors, I declare that this work is original, has not been published previously, and is not under consideration for publication elsewhere, in whole or in part. All listed authors have reviewed and approved the enclosed manuscript.

Acknowledgments

This paper has been financially supported by the National Natural Science Foundation of China (No. 52374063), Shandong Provincial Natural Science Foundation, China (Nos. ZR2024QE075, ZR2023ME049, ZR2025MS902), the Fundamental Research Funds for the Central Universities (Nos. 24CX06017A, 25CX07004A).

References

Arshad, A., Al-Majed, A.A., Menouar, H., et al., 2009. Carbon dioxide (CO_2) miscible flooding in tight oil reservoirs: A case study. In: SPE Kuwait International Petroleum Conference and Exhibition. https://doi.org/10.2118/127616-MS.
Beven, K., Germann, P., 2013. Macropores and water flow in soils revisited. Water Resour. Res. 49 (6), 3071–3092. https://doi.org/10.1002/wrcr.20156.
Blatt, H., Middleton, G.V., Murray, R.C., 1980. Origin of Sedimentary Rocks. Prentice-Hall, Englewood Cliffs.
Cai, M.Y., Su, Y.L., Hao, Y.M., et al., 2021. Monitoring oil displacement and CO_2 trapping in low-permeability media using NMR: A comparison of miscible and immiscible flooding. Fuel 305, 121606. https://doi.org/10.1016/j.fuel.2021.121606.
Chen, H., Liu, X.L., Zhang, C., et al., 2022. Effects of miscible degree and pore scale on seepage characteristics of unconventional reservoirs fluids due to supercritical CO_2 injection. Energy 239, 122287. https://doi.org/10.1016/j.energy.2021.122287.
Clarke, R.H., 1979. Reservoir properties of conglomerates and conglomeratic sandstones: Geologic notes. AAPG (Am. Assoc. Pet. Geol.) Bull. 63 (5), 799–803. https://doi.org/10.1306/2F9182D9-16CE-11D7-8645000102C1865D.
Cnudde, V., Boone, M.N., 2013. High-resolution X-ray computed tomography in geosciences: A review of the current technology and applications. Earth Sci. Rev. 123, 1–17. https://doi.org/10.1016/j.earscirev.2013.04.003.
Coates, G.R., Xiao, L., Prammer, M.G., 1999. NMR Logging Principles and Applications. Halliburton Energy Services, Houston.
Cronin, B.T., Kidd, R.B., 1998. Heterogeneity and lithotype distribution in ancient deep-sea canyons: point Lobos deep-sea canyon as a reservoir analogue. Sediment. Geol. 115 (1), 315–349. https://doi.org/10.1016/S0037-0738(97)00099-7.
Du, D.J., Pu, W.F., Jin, F.Y., et al., 2020. Experimental study on EOR by CO_2 huff-n-puff and CO_2 flooding in tight conglomerate reservoirs with pore scale. Chem. Eng. Res. Des. 156, 425–432. https://doi.org/10.1016/j.cherd.2020.02.018.
Ghasemi, M., Astutik, W., Alavian, S., et al., 2017. Tertiary-CO_2 flooding in a composite fractured-chalk reservoir. In: SPE Reservoir Characterisation and

Simulation Conference and Exhibition, SPE-186046-MS. https://doi.org/10.2118/186046-MS.
Guo, J.C., Zhou, H.Y., Zeng, J., et al., 2020. Advances in low-field nuclear magnetic resonance (NMR) technologies applied for characterization of pore space inside rocks: A critical review. Pet. Sci. 17 (5), 1281–1297. https://doi.org/10.1007/s12182-020-00488-0.
Han, H.S., Li, S., Ma, D.S., et al., 2018. Investigation of flue gas displacement and storage after the water flooding in a full diameter conglomerate long-core. Petrol. Explor. Dev. 45 (5), 903–909. https://doi.org/10.1016/S1876-3804(18)30093-4.
Iraji, B., Shadizadeh, S.R., Riazi, M., 2015. Experimental investigation of CO_2 huff and puff in a matrix-fracture system. Fuel 158, 105–112. https://doi.org/10.1016/j.fuel.2015.04.069.
Iyer, J., Lackey, G., Edvardsen, L., et al., 2022. A review of well integrity based on field experience at carbon utilization and storage sites. Int. J. Greenh. Gas Control 113, 103533. https://doi.org/10.1016/j.ijggc.2021.103533.
Jia, H.B., Ji, H.C., Wang, L.S., et al., 2017. Reservoir quality variations within a conglomeratic fan-delta system in the Mahu Sag, northwestern Junggar Basin: Characteristics and controlling factors. J. Petrol. Sci. Eng. 152, 165–181. https://doi.org/10.1016/j.petrol.2017.03.002.
Jia, C.Z., Zou, C.N., Yang, Z., et al., 2018. Significant progress of continental petroleum geological theory in basins of central and Western China. Petrol. Explor. Dev. 45 (4), 573–588. https://doi.org/10.1016/S1876-3804(18)30064-8.
Kim, K.Y., Oh, J., Han, W.S., et al., 2018. Two-phase flow visualization under reservoir conditions for highly heterogeneous conglomerate rock: A core-scale study for geologic carbon storage. Sci. Rep. 8 (1), 4869. https://doi.org/10.1038/s41598-018-23224-6.
Koray, A.M., Appiah Kubi, E., Bui, D., et al., 2025. Cost-effective strategies for assessing CO_2 water-alternating-gas (WAG) injection for enhanced oil recovery (EOR) in a heterogeneous reservoir. Water 17 (5), 651. https://doi.org/10.3390/w17050651.
Li, S.Y., Wang, Q., Zhang, K.Q., et al., 2020. Monitoring of CO_2 and CO_2 oil-based foam flooding processes in fractured low-permeability cores using nuclear magnetic resonance (NMR). Fuel 263, 116648. https://doi.org/10.1016/j.fuel.2019.116648.
Li, Y.W., Yang, Y.F., Dong, M.Z., et al., 2024. Pore-scale characterization of CO_2 trapping and oil displacement in three-phase flow in a heterogeneous layered sandstone. SPE J. 29 (2), 1147–1160. https://doi.org/10.2118/217996-PA.
Liu, Z.Y., Li, Y.Q., Leng, R.X., et al., 2020. Effects of pore structure on surfactant/polymer flooding-based enhanced oil recovery in conglomerate reservoirs. Petrol. Explor. Dev. 47 (1), 134–145. https://doi.org/10.1016/S1876-3804(20)60012-X.
Liu, J.R., Li, H.Y., Tan, Q.Z., et al., 2022. Quantitative study of CO_2 huff-n-puff enhanced oil recovery in tight formation using online NMR technology. J. Petrol. Sci. Eng. 216, 110688. https://doi.org/10.1016/j.petrol.2022.110688.
Liu, X.L., Chen, H., Cheng, W.M., et al., 2025a. Occurrence states and transport behavior of crude oil in different permeability oil reservoirs during depletion development. Geoenergy Sci. Eng. 252, 213944. https://doi.org/10.1016/j.geoen.2025.213944.
Liu, X.L., Chen, H., Li, Y., et al., 2025b. Oil production characteristics and CO_2 storage mechanisms of CO_2 flooding in ultra-low permeability sandstone oil reservoirs. Petrol. Explor. Dev. 52 (1), 196–207. https://doi.org/10.1016/S1876-3804(25)60014-0.
Luo, Y.C., Xiao, H.M., Liu, X.G., et al., 2023. Diffusion coefficient and the volume swelling of CO_2/light oil systems: Insights from dynamic volume analysis and molecular dynamics simulation. J. Mol. Liq. 382, 121943. https://doi.org/10.1016/j.molliq.2023.121943.
Pu, W.F., Wei, B., Jin, F.Y., et al., 2016. Experimental investigation of CO_2 huff-n-puff process for enhancing oil recovery in tight reservoirs. Chem. Eng. Res. Des. 111, 269–276. https://doi.org/10.1016/j.cherd.2016.05.012.
Ramachandran, K.P., Gyani, O.N., Sur, S., 2010. Immiscible hydrocarbon wag: Laboratory to field. In: SPE Oil and Gas India Conference and Exhibition. https://doi.org/10.2118/128848-MS.
Raza, A., Glatz, G., Gholami, R., et al., 2022. Carbon mineralization and geological storage of CO_2 in basalt: Mechanisms and technical challenges. Earth Sci. Rev. 229, 104036. https://doi.org/10.1016/j.earscirev.2022.104036.
Rezk, G.M., Foroozesh, J., 2022. Uncertainty effect of CO_2 molecular diffusion on oil recovery and gas storage in underground formations. Fuel 324, 124770. https://doi.org/10.1016/j.fuel.2022.124770.
Song, Y.L., Song, Z.J., Chen, Z.X., et al., 2024. Simulation of CO_2 enhanced oil recovery and storage in shale oil reservoirs: Unveiling the impacts of nano-confinement and oil composition. Adv. Geo-Energy Res. 13 (2), 106–118. https://doi.org/10.46690/ager.2024.08.05.
Tan, L., Zhang, J.G., Zhang, J., et al., 2025. Study on the propagation law of CO_2 displacement in tight conglomerate reservoirs in the Mahu Depression, Xinjiang, China. Energies 18 (4), 990. https://doi.org/10.3390/en18040990.
Udden, J.A., 1914. Mechanical composition of clastic sediments. Bull. Geol. Soc. Am. 25 (1), 655–744. https://doi.org/10.1130/GSAB-25-655.
Wang, J.K., Zhang, Y.P., Xie, J., 2020. Influencing factors and application prospects of CO_2 flooding in heterogeneous glutenite reservoirs. Sci. Rep. 10 (1), 1839. https://doi.org/10.1038/s41598-020-58792-z.
Wei, B., Zhang, X., Wu, R.N., et al., 2019. Pore-scale monitoring of CO_2 and N_2 flooding processes in a tight formation under reservoir conditions using nuclear magnetic resonance (NMR): A case study. Fuel 246, 34–41. https://doi.org/10.1016/j.fuel.2019.02.103.
Wei, B., Liu, J., Zhang, X., et al., 2020. Nuclear Magnetic Resonance (NMR) mapping of remaining oil distribution during sequential rate waterflooding processes for improving oil recovery. J. Petrol. Sci. Eng. 190, 107102. https://doi.org/10.1016/j.petrol.2020.107102.
Wei, J.G., Zhang, D., Zhang, X., et al., 2023. Experimental study on water flooding mechanism in low permeability oil reservoirs based on nuclear magnetic resonance technology. Energy 278, 127960. https://doi.org/10.1016/j.energy.2023.127960.
Wentworth, C.K., 1922. A scale of grade and class terms for clastic sediments. J. Geol. 30 (5), 377–392. https://doi.org/10.1086/622910.
Wildenschild, D., Sheppard, A.P., 2013. X-ray imaging and analysis techniques for quantifying pore-scale structure and processes in subsurface porous medium systems. Adv. Water Resour. 51, 217–246. https://doi.org/10.1016/j.advwatres.2012.07.018.
Xu, C.F., Liu, H.X., Qian, G.B., et al., 2011. Microcosmic mechanisms of water-oil displacement in conglomerate reservoirs in Karamay Oilfield, NW China. Petrol. Explor. Dev. 38 (6), 725–732. https://doi.org/10.1016/S1876-3804(12)60006-8.
Xu, L., Myers, M., Li, Q., et al., 2020. Migration and storage characteristics of supercritical CO_2 in anisotropic sandstones with clay interlayers based on X-CT experiments. J. Hydrol. 580, 124239. https://doi.org/10.1016/j.jhydrol.2019.124239.
Yang, Y.B., Peng, X., Xiao, W.L., et al., 2025. The effect of the displacement pressure on migration of fluid during the imbibition for tight oil reservoir. Sci. Rep. 15 (1), 23768. https://doi.org/10.1038/s41598-025-07636-9.
Zhang, T., Tang, M., Ma, Y.K., et al., 2022. Experimental study on CO_2/Water flooding mechanism and oil recovery in ultralow—Permeability sandstone with online LF-NMR. Energy 252, 123948. https://doi.org/10.1016/j.energy.2022.123948.
Zhang, Z.X., Ge, H.K., Wang, J.B., et al., 2023. Influence of gravel content and cement on conglomerate fracture. Pet. Sci. 20 (3), 1724–1741. https://doi.org/10.1016/j.petsci.2023.03.027.
Zhang, M.Y., Li, B.F., Xin, Y., et al., 2025a. Experimental study on CO_2 flooding in tight sandy conglomerate cores: Oil displacement and CO_2 storage. Energy 333, 137336. https://doi.org/10.1016/j.energy.2025.137336.
Zhang, X.Y., Xu, R., Zhao, Q., et al., 2025b. Enhanced oil recovery in reservoirs via diffusion-driven CO_2 flooding: Experimental insights and material balance modeling. Phys. Fluids 37 (8). https://doi.org/10.1063/5.0279982.
Zhou, X., Yuan, Q.W., Zhang, Y.Z., et al., 2019. Performance evaluation of CO_2 flooding process in tight oil reservoir via experimental and numerical simulation studies. Fuel 236, 730–746. https://doi.org/10.1016/j.fuel.2018.09.035.
Zhao, Z.W., Zhang, S.C., Zou, Y.S., et al., 2024. Evaluation of gas flooding effect in Mahu tight sandstone reservoir. In: ARMA US Rock Mechanics/Geomechanics Symposium, ARMA-2024-0741. https://doi.org/10.56952/ARMA-2024-0741.
Zhou, X.M., Yu, W., Lei, G., et al., 2024. Experimental study on dual benefits of improvement of CO_2 enhanced oil recovery and its storage capacity for depleted carbonate oil reservoirs. Adv. Geo-Energy Res. 12 (1), 52–65. https://doi.org/10.46690/ager.2024.04.05.